J|A|C|S
ARTICLES
Published on Web 03/06/2004

Mechanisms of HNO and NO Production from Angeli's Salt: Density Functional and CBS-QB3 Theory Predictions

Andrew S. Dutton,[†] Jon M. Fukuto,[‡] and K. N. Houk*,[†]

Contribution from the Department of Chemistry and Biochemistry, University of California, Los Angeles, California 90095-1569, and Department of Pharmacology, School of Medicine, Center for the Health Sciences, University of California, Los Angeles, California 90095-1735

Received October 21, 2003; E-mail: houk@chem.ucla.edu

Abstract: The mechanism of decomposition of Angeli's salt, $Na_2N_2O_3$, was explored with B3LYP and CBS-QB3 computational methods. Angeli's salt produces both nitroxyl (HNO) and nitric oxide (NO), depending upon the pH of the solution. These calculations show that protonation on N(2), while less favorable than O protonation, leads spontaneously to HNO production, while diprotonation at O(3) leads to NO generation. K_a values for protonation at different centers and rate constants have been found which reproduce experimental data satisfactorily.

Introduction

Angeli's salt, $Na_2N_2O_3$, variously called sodium trioxodinitrate(II), oxyhyponitrate, *N*-nitrohydroxylamate, or hyponitrate, was first prepared in the late 19th century.[1] The synthesis was refined in 1952.[2] The structure of this molecule was the subject of much debate[2−7] and eluded chemists until the crystal structure was determined in 1973.[7] Angeli's salt decomposes thermally or in aqueous solutions to give several different nitrogen oxides depending upon the conditions.[1,8]

Figure 1 summarizes the investigations by Hughes and Wimbledon on the pH dependence of the rate constants for decomposition of Angeli's salt.[9] The products of aqueous decomposition are highly pH dependent; HNO is generated and quickly dimerizes to give N_2O in the pH range of 8−4, while NO is produced in solutions with a pH less than 4. Angeli's salt is quite stable in basic solution (pH > 10). The rate of decomposition increases with decreasing pH and becomes pH independent in the range of pH 8−4. Below pH 4, the rate increases dramatically.

The mechanism for decomposition has been of much interest, and a variety of proposals have been put forth. Angeli proposed that the decomposition of $Na_2N_2O_3$ to form nitrite and N_2O involved cleavage of the N−N bond to produce HNO that subsquently dimerizes and loses water to form N_2O.[1] Hendrickson and co-workers used isotopically labeled nitrogen to demonstrate that the nitrogen of the nitrite product comes from N(1), the nitrogen bearing the two oxygens in Angeli's salt.[5] Bonner et al., using ^{15}N NMR experiments, and Bazylinski et al., utilizing ^{15}NO to trap HNO, proposed that decomposition in neutral pH would occur through protonation at N(2), yielding NO^-, based upon the erroneous pK_a of 4.7 for HNO, and nitrite.[11,12] Using a hemoglobin detection system, Doyle and co-workers suggest that decomposition produces NO and $HONO^-$.[14] The mechanism for the production of NO is still unknown but is generally thought to involve HNO_2, a byproduct of HNO production, and is not simply a dehydration process.[7−14]

HNO has physiological functions that are proposed to differ from those of other nitrogen oxides, but the elusiveness of HNO

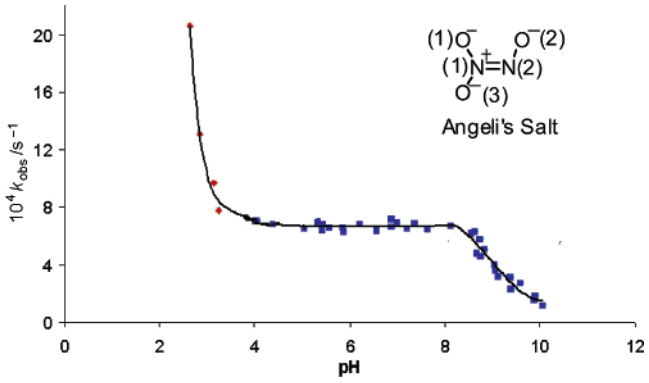

Figure 1. Plot of the rate constants of decomposition of Angeli's salt versus pH from Hughes and Wimbledon.[9] The ■ show the rate of the disappearance of Angeli's salt to yield nitrite (NO_2^-), and ◆ show the rate of the disappearance of Angeli's salt to give nitric oxide (NO).

[†] Department of Chemistry and Biochemistry.
[‡] Department of Pharmacology, School of Medicine, Center for the Health Sciences.

(1) Angeli, A. *Gazz. Chim. Ital*. **1896**, *26*, 17.
(2) Addison, C. C.; Gamlen, G. A.; Thompson, R. *J. Chem. Soc.* **1952**, 339.
(3) (a) Hunt, H. R., Jr.; Cox, J. R., Jr.; Ray, J. D. *Inorg. Chem.* **1962**, *1*, 938. (b) Sturrock, P. E.; Ray, J. D.; McDowell, J.; Hunt, H. R., Jr. *Inorg. Chem.* **1963**, *2*, 649.
(4) Feltham, R. D. *Inorg. Chem.* **1964**, *3*, 900.
(5) Hendrickson, D. N.; Jolly, W. L. *Inorg. Chem.* **1969**, *8*, 693.
(6) Hendrickson, D. N.; Hollander, J. M.; Jolly, W. L. *Inorg. Chem.* **1969**, *8*, 2642.
(7) Hope, H.; Sequeira, M. R. *Inorg. Chem.* **1973**, *12*, 286−288.
(8) Oza, T. M. *J. Chem. Soc. A* **1968**, 2441−2444.
(9) Hughes, M. N.; Wimbledon, P. E. *J. Chem. Soc., Dalton Trans.* **1976**, 703−707.
(10) Bonner, F. T.; Ravid, B. *Inorg. Chem.* **1975**, *14*, 558−563.
(11) Cambi, L. *Ber. Dtsch. Chem. Ges. B* **1936**, *69*, 2027.
(12) Bonner, F. T.; Degani, H.; Akhtar, M. J. *J. Am. Chem. Soc.* **1981**, *103*, 3739−3742.
(13) Bazylinski, D. A.; Hollocher, T. C. *Inorg. Chem.* **1985**, *24*, 4285−4288.
(14) Doyle, M. P.; Mahapatro, S. N. *J. Am. Chem. Soc.* **1984**, *106*, 3678−3679.

makes it difficult to identify its biochemistry. HNO rapidly dimerizes and decomposes via dehydration to yield nitrous oxide, N_2O, with a second-order rate constant of 8×10^6 M^{-1} s^{-1}.[15]

Recently, there have been conflicting reports regarding the use of Angeli's salt as a source for HNO in aerobic biochemical studies.[16−18] Some workers have raised the possibility that peroxynitrite, $ONOO^-$, is produced from Angeli's salt. The most recent report[16] indicates that HNO is indeed produced from Angeli's salt decomposition by demonstrating that compounds that react with HNO increase the rate of decomposition. Liochev and Fridovich also suggest that the $ONOO^-$ that is observed experimentally occurs from the reaction of HNO/NO^- with O_2 with a rate constant of 8×10^3 M^{-1} s^{-1}. Miranda et al. have estimated a value of 3×10^3 M^{-1} s^{-1} for the rate constant of reaction of HNO/NO^- with O_2.[19]

Biological experiments utilizing Angeli's salt demonstrate that the decomposition products are toxic, capable of causing glutathione depletion and double-stranded DNA breaks.[20] In mammalian cells, HNO is toxic only in the presence of oxygen.[20,21] It is thought that HNO reacts with oxygen to form an as-yet unidentified oxidant that does not appear to be peroxynitrite.[20] In contrast to the widely known function of NO, arterial dilation, HNO causes venodilation while not affecting the heart rate.[22]

We have undertaken a theoretical study of the mechanism of decomposition of Angeli's salt to form HNO and NO, as well as an estimation of the basicities of various species involved in the decomposition pathway. The reaction mechanism is complementary to our recent calculations of the mechanism of the decomposition of dialkylamino diaziumdiolates, which form NO exclusively.[23]

Methods

All structures were optimized using the B3LYP method with a 6-311+G(d) basis set using the Gaussian 98 program.[24] Structures that required more accurate energy calculations were recomputed by CBS-QB3, a series of calculations that generally give energies within ±1 kcal/mol of experimentally measured values for the G3 data set.[25] Free energies were given for 298 K. Aqueous solvation energies were calculated as single points on the B3LYP/6-311+G(d) optimized geometries using a 6-311+G(d) basis set in the PCM model, implemented in Gaussian 98. The solvation energies were applied to the B3LYP/6-311+G(d) and CBS-QB3 optimized gas-phase energies. Key structures to the decomposition mechanism were optimized in water using the PCM model[26] and basis set mentioned above to better simulate the solvent effects on the mechanism utilizing Gaussian 03.[27] All values reported in the text are at the CBS-QB3 level of theory unless otherwise noted. The relative pK_a values were predicted using the relationship between $\Delta\Delta G_{aq}$ and pK_a, $\Delta G = 1.36(pK_a)$ at 25 °C. The most basic computed pK_a was set equal to the experimentally measured pK_a values of 9.3 and 2.5 for pK_1 and pK_2, respectively.[3b,9] The monoprotonated species were computed relative to pK_1, and the diprotonated species were computed relative to pK_2.

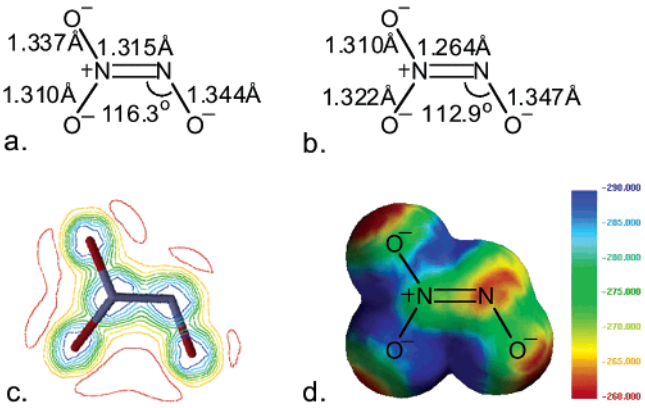

Figure 2. Comparison of the structural details between the computed and the X-ray crystal structure, distances given in Å, along with the computed electrostatic potential. (a) B3LYP/6-311+G(d). (b) The X-ray crystal structure.[7] (c) A cross-sectional view of the electrostatic potential. (d) The electrostatic potential projected onto an electronic isodensity surface. The scale shows the difference in electrostatic potential, with red representing areas of large negative charge densities.

Results and Discussion

Figure 2 shows (a) the computed structure of the dianion, O_2NNO^{2-}, (b) the X-ray crystal structure[7] of the $N_2O_3^{2-}$ unit in the disodium monohydrate, and (c and d) two electrostatic potential representations of the dianion.

The computed and X-ray structures are quite similar, considering that the crystal structure contains counterions and a molecule of water. The NN bond distance has the largest discrepancy of 0.051 Å. The largest bond angle difference of

(15) Shafirovich, V.; Lymar, S. V. *Proc. Natl. Acad. Sci. U.S.A.* **2002**, *99*, 7340−7345.
(16) Liochev, S. I.; Fridovich, I. *Free Radical Biol. Med.* **2003**, *34*, 1399 and references therein.
(17) Reardon, P.; Beckman, J. *Free Radical Biol. Med.* **2002**, *33* (Suppl. 2), 380.
(18) Beckman, J. S.; Reardon, P. *Free Radical Biol. Med.* **2002**, *33* (Suppl. 1), 3.
(19) Miranda, K. M.; Paolocci, N.; Katori, T.; Douglas, D. T.; Ford, E.; Bartberger, M.; Espey, M. G.; Kass, D. A.; Feelisch, M.; Fukuto, J. M.; Wink, D. A. *Proc. Natl. Acad. Sci. U.S.A.* **2003**, *100*, 9196−9201.
(20) Wink, D. A.; Feelisch, M.; Fukuto, J.; Chistodoulou, D.; Jourd'heuil, D.; Grisham, M. B.; Vodovotz, Y.; Cook, J. A.; Krishna, M.; Degraff, W. G.; SungMee, K.; Gamson, J.; Mitchell, J. B. *Arch. Biochem. Biophys.* **1998**, *351*, 66−74.
(21) Miranda, K. M.; Espey, M. G.; Yamada, K.; Krishna, M.; Ludwick, N.; SungMee, K.; Jourd'heuil, D.; Grisham, M. B.; Feelisch, M.; Fukuto, J. M.; Wink, D. A. *J. Biol. Chem.* **2001**, *276*, 1720−1727.
(22) Paolocci, N.; Saaverdra, W. F.; Miranda, K. M.; Martignani, C.; Isoda, T.; Hare, J. M.; Espey, M. G.; Fukuto, J. M.; Feelisch, M.; Wink, D. A.; Kass, D. A. *Proc. Natl. Acad. Sci. U.S.A.* **2001**, *98*, 10463−10468.
(23) Dutton, A. S.; Fukuto, J. M.; Houk, K. N. *Inorg. Chem.* **2004**, *43*, 1039−1045.
(24) Frisch, M. J.; Trucks, G. W.; Schlegel, H. B.; Scuseria, G. E.; Robb, M. A.; Cheeseman, J. R.; Zakrzewski, V. G.; Montgomery, J. A., Jr.; Stratmann, R. E.; Burant, J. C.; Dapprich, S.; Millam, J. M.; Daniels, A. D.; Kudin, K. N.; Strain, M. C.; Farkas, O.; Tomasi, J.; Barone, V.; Cossi, M.; Cammi, R.; Mennucci, B.; Pomelli, C.; Adamo, C.; Clifford, S.; Ochterski, J.; Petersson, G. A.; Ayala, P. Y.; Cui, Q.; Morokuma, K.; Malick, D. K.; Rabuck, A. D.; Raghavachari, K.; Foresman, J. B.; Cioslowski, J.; Ortiz, J. V.; Stefanov, B. B.; Liu, G.; Liashenko, A.; Piskorz, P.; Komaromi, I.; Gomperts, R.; Martin, R. L.; Fox, D. J.; Keith, T.; Al-Laham, M. A.; Peng, C. Y.; Nanayakkara, A.; Gonzalez, C.; Challacombe, M.; Gill, P. M. W.; Johnson, B. G.; Chen, W.; Wong, M. W.; Andres, J. L.; Head-Gordon, M.; Replogle, E. S.; Pople, J. A. *Gaussian 98*, revision A.1; Gaussian, Inc.: Pittsburgh, PA, 1998.
(25) Montgomery, J. A.; Ochterski, J. W.; Peterson, G. A. *J. Chem. Phys.* **1994**, *101*, 5900.
(26) Cossi, M.; Barone, R.; Cammi, R.; Tomasi, J. *Chem. Phys. Lett.* **1996**, *255*, 327.
(27) Frisch, M. J.; Trucks, G. W.; Schlegel, H. B.; Scuseria, G. E.; Robb, M. A.; Cheeseman, J. R.; Montgomery, J. A., Jr.; Vreven, T.; Kudin, K. N.; Burant, J. C.; Millam, J. M.; Iyengar, S. S.; Tomasi, J.; Barone, V.; Mennucci, B.; Cossi, M.; Scalmani, G.; Rega, N.; Petersson, G. A.; Nakatsuji, H.; Hada, M.; Ehara, M.; Toyota, K.; Fukuda, R.; Hasegawa, J.; Ishida, M.; Nakajima, T.; Honda, Y.; Kitao, O.; Nakai, H.; Klene, M.; Li, X.; Knox, J. E.; Hratchian, H. P.; Cross, J. B.; Adamo, C.; Jaramillo, J.; Gomperts, R.; Stratmann, R. E.; Yazyev, O.; Austin, A. J.; Cammi, R.; Pomelli, C.; Ochterski, J. W.; Ayala, P. Y.; Morokuma, K.; Voth, G. A.; Salvador, P.; Dannenberg, J. J.; Zakrzewski, V. G.; Dapprich, S.; Daniels, A. D.; Strain, M. C.; Farkas, O.; Malick, D. K.; Rabuck, A. D.; Raghavachari, K.; Foresman, J. B.; Ortiz, J. V.; Cui, Q.; Baboul, A. G.; Clifford, S.; Cioslowski, J.; Stefanov, B. B.; Liu, G.; Liashenko, A.; Piskorz, P.; Komaromi, I.; Martin, R. L.; Fox, D. J.; Keith, T.; Al-Laham, M. A.; Peng, C. Y.; Nanayakkara, A.; Challacombe, M.; Gill, P. M. W.; Johnson, B.; Chen, W.; Wong, M. W.; Gonzalez, C.; Pople, J. A. *Gaussian 03*, revision B.04; Gaussian, Inc.: Pittsburgh, PA, 2003.

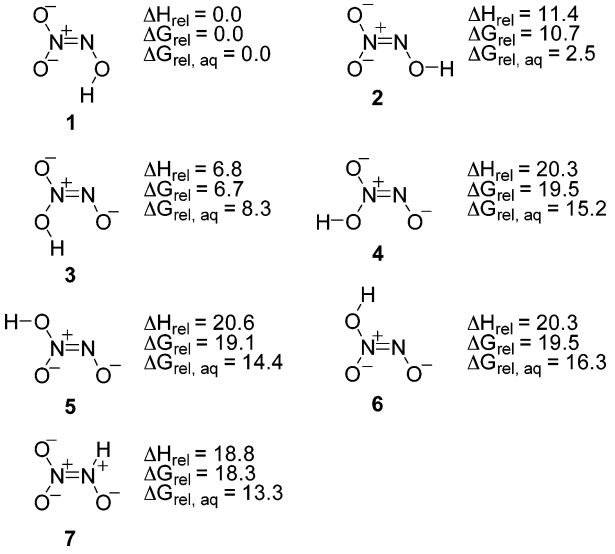

Figure 3. Relative energies in kcal/mol of the monoprotonated species (CBS-QB3, PCM (B3LYP/6-311+G(d))).

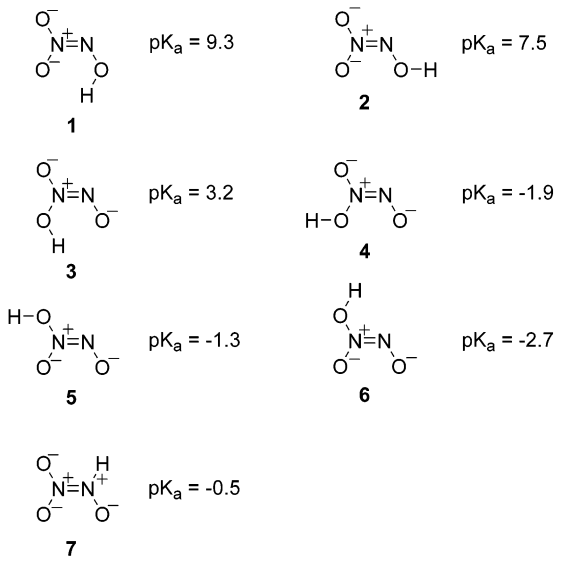

Figure 4. Computed pK_a values (CBS-QB3, PCM (B3LYP/6-311+G(d))).

3.4° involves the O(3)N(2)N(1) bond angle. Both structures are planar. The electrostatic potential, shown in Figure 2, and the natural bond orbital (NBO) analysis of the atomic charges suggests that all of the oxygens and N(2) are sites of high electron density.

All monoprotonated species derived from Angeli's salt were optimized. The results are shown in Figure 3. Energies are relative values of ΔH (electronic energy + ZPE + thermal corrections), ΔG values for 298 K in the gas phase, and ΔG_{aq}, which include aqueous solvation energies computed by the PCM method.

The most thermodynamically favored position for protonation is the oxygen of the nitroso group, structure **1**. The non-hydrogen bonded conformer, structure **2**, is much higher in energy in the gas phase, but only 2.5 kcal/mol higher in water. Protonation of O(1) gives the hydrogen-bonded structure **3** that is between **1** and **2** in energy in the gas phase. The non-hydrogen-bonded conformer of this, **4**, is much higher in energy, as are the products of protonation at O(3), **5** and **6**. Protonation of N(2) gives structure **7**, which is 13.3 kcal/mol higher in energy in water than structure **1**. The stabilization effect of hydrogen bonding, 10−15 kcal/mol in the gas phase, but only 2.5−6.0 kcal/mol in water, is illustrated by comparing the energies of structures **1** to **2** and of **3** to **4**.

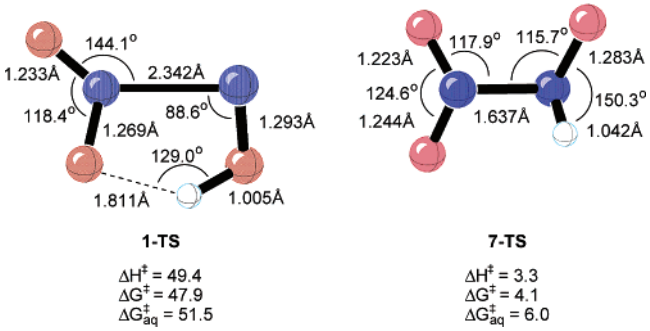

Figure 5. Transition-state geometries and activation energetics in kcal/mol (B3LYP/6-311+G(d), PCM (B3LYP/6-311+G(d))).

The pK_a's of Angeli's salt have been measured experimentally to be 2.51 and 9.7, via extrapolation to an ionic strength of zero, by Hunt and co-workers,[3b] and >3 and 9.35 at an ionic strength of 0.25 mol dm^{-3} by Hughes et al.[9] Setting the pK_a of the least acidic tautomer, **1**, to 9.3 and using the computed relative free energies in water, theoretically calculated pK_a's are derived and shown in Figure 4. The trend in basicity follows that of the relative energetics shown in Figure 3, with **1** being the most basic and **6** being the least. The calculated pK_a's for structures **1** and **7** are 9.3 and −0.5, respectively.

We have explored the reactivities of the monoprotonated species **1**, **6**, and **7**. The transition states for N−N cleavage of **1** (**1-TS**) and **7** (**7-TS**) were located in the gas phase, and single-point energetics were evaluated with the PCM model to obtain aqueous solvation energies. The transition structures and their energetics are shown in Figure 5, and the reaction energetics are summarized in eqs 1−3.

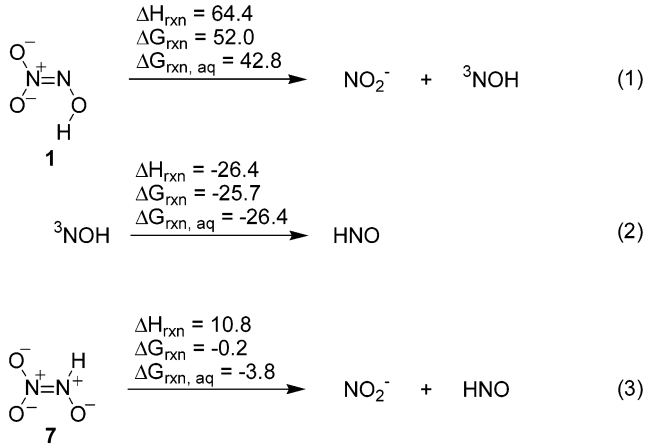

Decomposition of **1** is very unfavorable and gives the high energy intermediate, NOH, as shown in eq 1. NOH, a ground-state triplet, possesses a singlet−triplet gap of 15.7 kcal/mol in water as calculated with the CBS-QB3 method. Equation 2 shows that the energy for the conversion of ^{3}NOH to HNO is −25.7 kcal/mol in the gas phase and −26.4 kcal/mol in water as calculated by CBS-QB3. These values agree well with the previous calculations[28,29] of −25.4 kcal/mol in the gas phase using MP2/6-311++** and −22.7 kcal/mol in the gas phase using CASPT2 with zero-point correction. This process has a

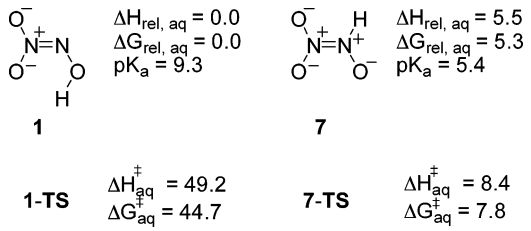

Figure 6. Relative energies in kcal/mol of species **1** and **7** optimized in water with computed pK_a values and transition-state energetics of species **1-TS** and **7-TS** optimized in water (B3LYP/6-311+G(d), PCM B3LYP/6-311+G(d)).

barrier of 56.2 and 53.8 kcal/mol in the gas and aqueous phases, respectively, using the B3LYP/6-311+G(d) method. The decomposition of **1** to HNO and NO_2^- is significantly endergonic, by 16.4 kcal/mol in water.

Species **7** has a very low barrier to decomposition, 7.8 kcal/mol in water. The reaction to form nitrite and HNO is slightly endothermic, but exergonic in the gas phase and water. An insignificant amount of **7** will be present at equilibrium, since the production of **7** from **1** involves a free-energy change of 5.3 kcal/mol. In the pH range from 8 to 4, Angeli's salt is primarily monoprotonated at the nitroso oxygen, species **1**, and the total free energy of activation for decomposition via the N-protonated species, **7**, is 13.1 kcal/mol. Attempts to find a transition state for decomposition of **3** led to proton transfer and a transition state the same as that found for decomposition of **1**.

Because of the importance of species **1** and **7** to the mechanism of decomposition, these structures as well as their transition states, **1-TS** and **7-TS**, respectively, were reoptimized in the PCM model of water to better simulate the experimental reaction conditions. The relative energies, theoretical pK_a values, and the energetics of the transition states are shown in Figure 6.

When the pH is lowered below a pH of 4, the products of decomposition change from HNO and NO_2^- to NO and HONO. The pH dependence implies that a diprotonated intermediate is involved. To determine the relative energies of diprotonated species, the structures resulting from protonating structures **1** through **7** were all optimized using the CBS-QB3 level of theory. The resulting relative gas-phase enthalpies, free energies, and the free energies in water are shown in Figure 7.

Calculations suggest that the monoprotonated species **1**, which will be present in the highest concentration, is most likely protonated a second time, leading to species **9** and **10**. The NO dimer plus water, **8**, is the most thermodynamically favored diprotonated product, arising from optimization of the O(3) diprotonated species. The molecular complex of water and the NO dimer is formed in the gas phase, but the energy to form the diprotonated species **8** is quite high, approximately 46.4 kcal/mol in water, as demonstrated by the bond-constrained structure **21** in Figure 8. A second protonation at O(1) of **3**, leading to species **14**, also results in spontaneous dissociation to water and the NO dimer, but the dimer is formed in an electronically

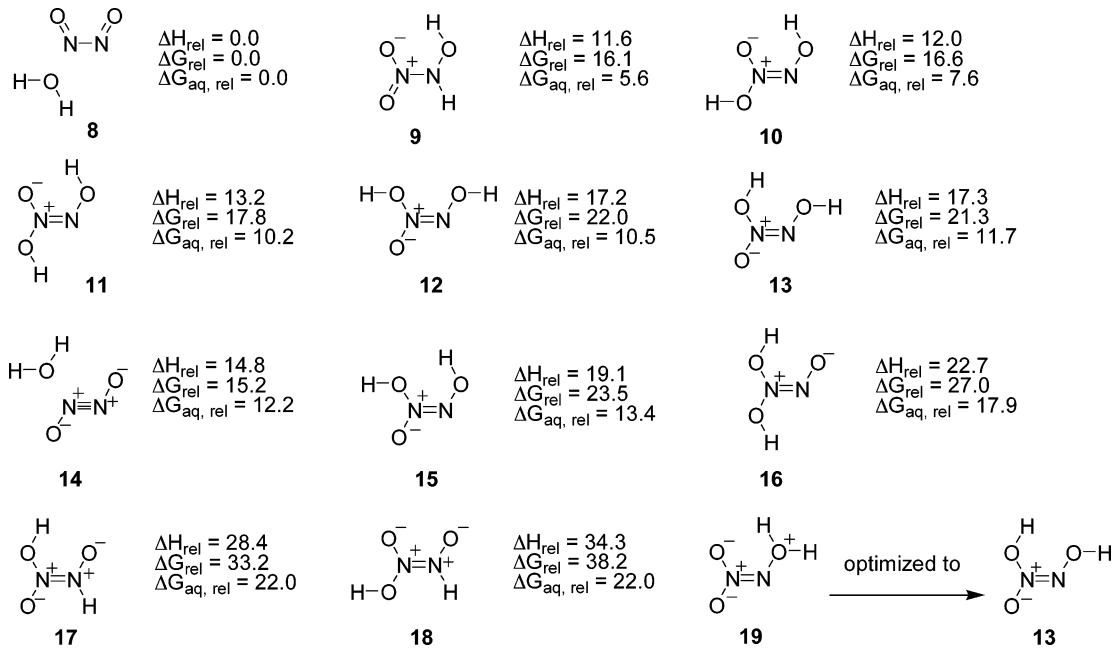

Figure 7. Relative energies in kcal/mol of the diprotonated species (CBS-QB3, PCM (B3LYP/6-311+G(d))). Attempted optimization of structure **19** gave **13**.

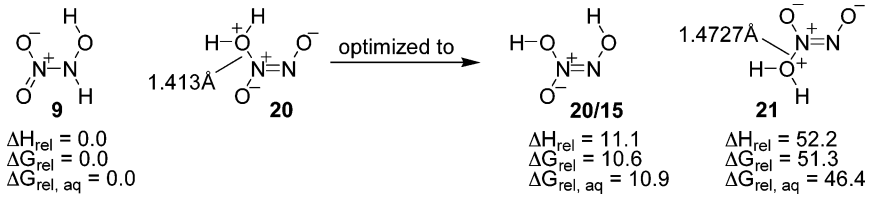

Figure 8. Relative energetics for the constrained bond structures of **8** and **14**. Changes in enthalpy and free energy in the gas phase and changes in the free energy in the aqueous phase in kcal/mol (B3LYP/6-311+G(d), PCM (B3LYP/6-311+G(d))).

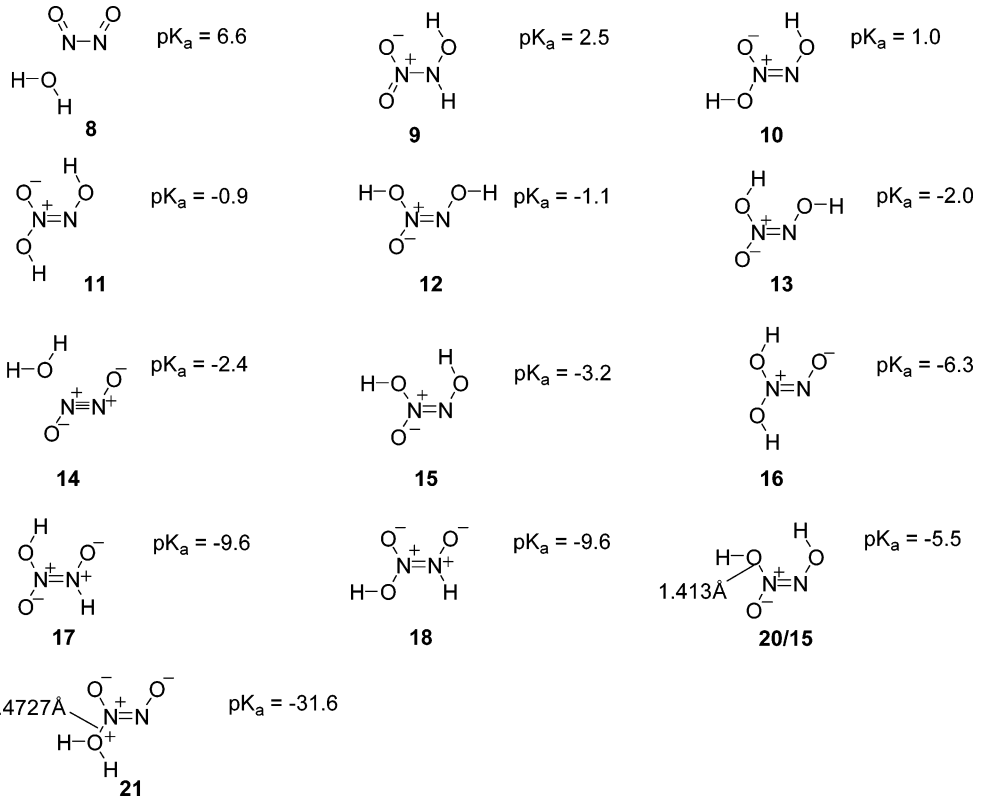

Figure 9. Computed pK_a values for the diprotonated species (structures **8**−**18** CBS-QB3, PCM (B3LYP/6-311+G(d)), structures **20/15** and **21** B3LYP/6-311+G(d), PCM (B3LYP/6-311+G(d))).

excited state which should relax rapidly to the trans dimer and then to two NO molecules. Similar results were found for the decomposition of the analogous isomer of dimethylamino diazeniumdiolate.[23]

The barrier to protonation and decomposition was approximated by constraining the O−N bond to the optimized monoprotonated bond length; this prevents dissociation. This was carried out for species **8**, constrained bond O(3)−N(1), and **14**, constrained bond O(1)−N(1), giving **21** and **20**, respectively. These are shown with their energies relative to species **9** in Figure 8. Interestingly, species **20** optimized to species **15**, indicating that once species **15** is formed, an internal hydrogen transfer leads to **20** which spontaneously decomposes to products. Attempts to find the concerted hydrogen transfer/decomposition transition state were unsuccessful, implying that there must be a very low barrier between species **15** and **14**.

Protonation of the protonated oxygen in species **1** leading to species **18** failed to give spontaneous dehydration, contrary to the other oxygen diprotonated species. Species **19** optimizes via proton transfer to species **13**, as shown in Figure 7.

The pK_a's for the diprotonated acids, shown in Figure 9, can be computed using the same method as in the monoprotonated cases; the pK_a of species **9** was set to the experimentally determined pK_a value of 2.5, and the other pK_a's were computed from the relative free energies in water shown in Figure 7.

Because the spontaneous decompositions of **8** and **14** could be due to the lack of favorable aqueous solvation during the optimization, the structures of **8**, **9**, **14**, and **20**/**15** were reoptimized in the PCM model for water. The oxygen-

Scheme 1. Proposed Mechanism for the Generation of HNO and NO from Angeli's Salt

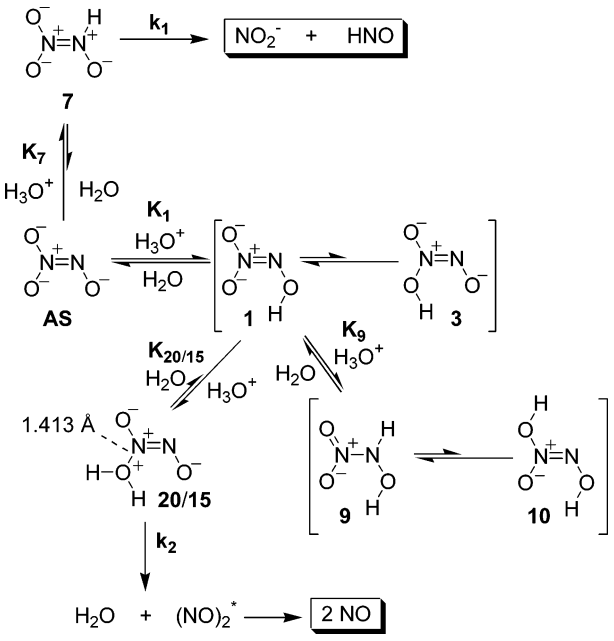

diprotonated species **8** and **14** spontaneously dissociated to the water and NO dimer molecular complex as seen in the earlier gas-phase optimizations. Optimization in aqueous solvent changed to the relative energy differences only slightly for structures **9** and **20**/**15**, as shown in Figure 10.

When the pH of the solution is lowered, such that the rate of diprotonation becomes competitive with $HN_2O_3^-$ decomposition, an equilibrium between the diprotonated species and the monoprotonated species will exist. From the relative energies

(28) Sumathi, R.; Peyerimhoff, S. D. *J. Chem. Phys.* **1997**, *107*, 1872−1880.
(29) Luna, A.; Merchan, M.; Roos, B. O. *Chem. Phys.* **1995**, *196*, 437−445.

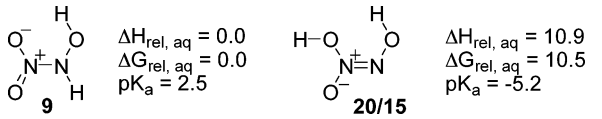

Figure 10. Relative energies (kcal/mol) of species **9** and **20/15** optimized in water with computed pK_a values (B3LYP/6-311+G(d), PCM B3LYP/6-311+G(d)).

in Figure 7, this equilibrium will favor the diprotic acid **9**. Species **9** is unreactive toward decomposition and will be in an equilibrium with the other diprotic acids. Species **20/15** with one oxygen diprotonated lies just 3.1 kcal/mol above **15** in water. Decomposition of **20** yields an electronically excited state of the NO dimer and water.[23] This excited state of the NO dimer will relax and dissociate to two molecules of NO. As seen by Cambi[11] and Hunt[3a] et al., when Angeli's salt is added to a 1 M solution of H_2SO_4 all the nitrogen is found as NO. This is in agreement with our proposed mechanism, shown in Scheme 1.

From the mechanism in Scheme 1, it is possible to derive a kinetic expression (eq 4) describing the rate of pH-dependent decomposition of Angeli's salt:

$$k_{obs} = [k_1K_1K_9K_{20/15}[H^+] + k_2K_7K_9[H^+]^2]/ [K_1K_7K_9K_{20/15} + K_7K_9K_{20/15}[H^+] + K_1K_9K_{20/15}[H^+] + K_7K_9[H^+]^2 + K_7K_{20/15}[H^+]^2] \quad (4)$$

In this equation, k_1 refers to the rate constant for the decomposition of **7** yielding HNO and nitrite and k_2 refers to the rate constant for decomposition of **20/15** to give water and an excited state of the trans NO dimer. K_1 and K_7 are the equilibrium constants for the monoprotonation of Angeli's salt giving species **1** and **7**, respectively, and K_9 and $K_{20/15}$ are the equilibrium constants for equilibium of **1** with the diprotonated species **9** and **20/15**, respectively.

By using these theoretical pK_a values and rate constants k_1 and k_2 as variables, it is possible to fit eq 4 to the experimental data from Hughes et al.[9] that was previously shown in Figure 1. The fit of computed to experimental data is shown is Figure 11. The theoretical rate constants k_1 and k_2 determined in this way are 5.2 s^{-1} and 1.7 $\times$ 10^5 s^{-1}, respectively.

The predicted rate constants in Scheme 1, k_1 and k_2, are in good qualitative agreement with the proposed mechanism in Scheme 1. From the computed transition state of species **7-TS** with a barrier of 7.8 kcal/mol when optimized in aqueous

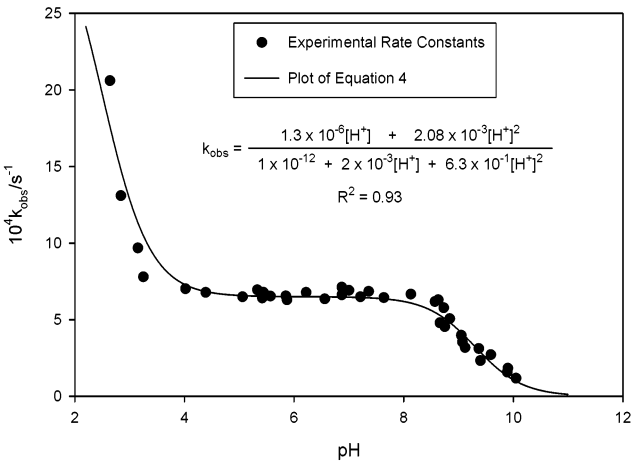

Figure 11. Dependence of the rate constant for decomposition of Angeli's salt on pH. The ● show the experimental rate constants[9] of the disappearance of Angeli's salt, and the line shows the fit of eq 4 to the experimental data utilizing computed pK_a values.

solvation and from the very low barrier to intramolecular proton transfer in going from species **15** to **14** via the intermediacy of species **15/20**, it is expected that k_1 is slower than k_2. These theoretical calculations suggest that as an aqueous solution of Angeli's salt is titrated with acid, Angeli's salt will be initially protonated to give an unreactive intermediate, species **1**, which will be in equilibrium with the reactive intermediate, species **7**, that decomposes with a rate of 5.2 s^{-1}, yielding HNO and nitrite. As the pH of the aqueous solution is lowered further, species **1** will become protonated again primarily at N(2) to give species **9**. This will be in equilibrium with species **20/15** that will rapidly lose water and form two molecules of NO with a rate constant of 1.7 $\times$ 10^5 s^{-1}.

Acknowledgment. We are grateful to the National Institute of General Medical Sciences, National Institutes of Health (K.N.H.), and the National Science Foundation (J.M.F.) for financial support of this research. A.S.D acknowledges the support of the National Institutes of Health, Chemistry and Biology Interface Training Grant from UCLA.

Supporting Information Available: Cartesian coordinates for all optimized structures and their energies (PDF). This material is available free of charge via the Internet at http://pubs.acs.org.

JA0391614